Nanocrystals

Ligand Crosslinking Boosts Thermal Transport in Colloidal Nanocrystal Solids

Zhongyong Wang, Arun Sundar S. Singaravelu, Rui Dai, Qiong Nian, Nikhilesh Chawla, and Robert Y. Wang*

Abstract: *The ongoing interest in colloidal nanocrystal solids for electronic and photonic devices necessitates that their thermal-transport properties be well understood because heat dissipation frequently limits performance in these devices. Unfortunately, colloidal nanocrystal solids generally possess very low thermal conductivities. This very low thermal conductivity primarily results from the weak van der Waals interaction between the ligands of adjacent nanocrystals. We overcome this thermal-transport bottleneck by crosslinking the ligands to exchange a weak van der Waals interaction with a strong covalent bond. We obtain thermal conductivities of up to 1.7 $Wm^{-1}K^{-1}$ that exceed prior reported values by a factor of 4. This improvement is significant because the entire range of prior reported values themselves only span a factor of 4 (i.e., 0.1–0.4 $Wm^{-1}K^{-1}$). We complement our thermal-conductivity measurements with mechanical nanoindentation measurements that demonstrate ligand crosslinking increases Young's modulus and sound velocity. This increase in sound velocity is a key bridge between mechanical and thermal properties because sound velocity and thermal conductivity are linearly proportional according to kinetic theory. Control experiments with non-crosslinkable ligands, as well as transport modeling, further confirm that ligand crosslinking boosts thermal transport.*

Introduction

Colloidal nanocrystals (NCs) are solution-grown, nanometer-sized, inorganic particles that are stabilized by a layer of molecular ligands attached to the particle surface. Upon deposition onto a substrate, these particles assemble into a solid material commonly referred to as a NC solid. NC solids have been used in a wide range of applications including electronics,[1] optoelectronics,[1a,2] photovoltaics,[3] and thermoelectrics.[4] Thermal properties of the active material play an important role in all of these applications. A high thermal conductivity is desired in electronics, optoelectronics, and photovoltaics because this minimizes the temperature rise
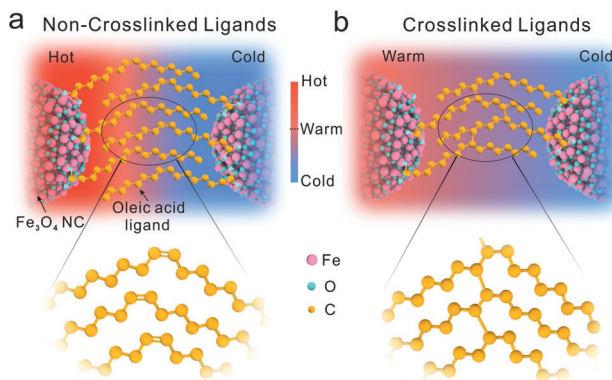
during device operation, and improves device performance and lifetime. On the other hand, a low thermal conductivity is desired in thermoelectric materials because this leads to large temperature gradients that are important to device function. Research on thermal transport in NC solids[5] shows that these materials have very low thermal conductivities of approximately 0.1–0.4 $Wm^{-1}K^{-1}$.[5] Although beneficial for thermoelectrics, this low thermal conductivity is problematic for the primary NC applications of interest, which include electronics, optoelectronics, and photovoltaics. Determining methods to obtain high thermal conductivity in these materials are consequently important.

Prior research on NC solids collectively point to the ligand chemistry as the main thermal-transport bottleneck.[5] These works studied the effect of varying ligand volume fraction in the NC solid by changing the NC size and/or exchanging the native ligands for shorter ligands.[5] Ong et al.[5a] showed that NC solid thermal conductivity is largely insensitive to the thermal conductivity of the NC core, which indicates that the NC–ligand interface and/or the ligand matrix is limiting thermal transport. Additional experiments by our group[5b] investigated a variety of NC–ligand binding groups, ligand lengths, and NC sizes. Our studies narrowed down the source of the low thermal conductivity to the ligand matrix itself. Within the ligand matrix, we identified the ligand–ligand interface between adjacent colloidal NCs as the key thermal-transport bottleneck.

In this work, we demonstrate that the thermal-transport bottleneck in NC solids can be overcome by crosslinking the molecular ligands on the NC surface through a moderate annealing treatment (Scheme 1). This ligand-crosslinking process effectively exchanges the weak van der Waals interactions with strong covalent bonds, and leads to a significant increase in thermal conductivity. We demonstrate this process on iron oxide NCs with oleic acid ligand molecules. Control experiments with non-crosslinkable stearic acid ligands confirm the impact of crosslinking on thermal transport. We complement our measurements of thermal conductivity with corresponding materials characterization, mechanical measurements, and thermal-transport modeling. Nanoindentation measurements demonstrate that crosslinking also increases Young's modulus and sound velocity. This increase in sound velocity is a key bridge between mechanical and thermal properties because sound velocity and thermal conductivity are linearly proportional according to kinetic theory.

[*] Z. Wang, A. S. S. Singaravelu, R. Dai, Prof. Q. Nian, Prof. N. Chawla, Prof. R. Y. Wang
School for Engineering of Matter, Transport & Energy
Arizona State University
Tempe, AZ 85281 (USA)
E-mail: rywang@asu.edu

Scheme 1. Schematic illustrations of ligand structure and the corresponding effect on thermal transport. The insets show zoomed-in views of the ligands before and after crosslinking (hydrogen atoms are omitted for improved clarity). a) Nanocrystal (NC) solids without ligand crosslinking have a low thermal conductivity and require large temperature gradients to move a given quantity of heat. This leads to a high temperature that is "hot" as represented by the bright-red background. b) After ligand crosslinking, NC solids have a high thermal conductivity and require smaller temperature gradients to move a given quantity of heat. This leads to a high temperature that is just "warm" as represented by the moderately red background.

Results and Discussion

We synthesized monodisperse 8–20 nm iron oxide NCs with either oleic acid (OA) ligands or stearic acid (SA) ligands by using a modified thermal-decomposition recipe.[6] Transmission electron microscopy (TEM) imaging and size

distribution histograms confirm uniform NC morphology and narrow size distributions (Figure S1). Thin films of NC solids were prepared by spin-coating and then heating to 150 °C to remove residual solvent. Figure 1 a–c and Figure S2 demonstrate that spin-coating results in ordered assemblies of iron oxide NCs. We crosslinked the ligands of adjacent NCs by using the heat treatment reported by Dreyer et al.[7] The crosslinking process is performed by heating the NC assembly to 350 °C for 30 minutes and is illustrated in Figure 1 d,e. The crosslinking process binds two adjacent ligands together by splitting the C=C double bond of the OA molecule into saturated C−C single bonds (Scheme 1).[7] This effectively exchanges the weak van der Waals interactions between neighboring ligands with strong covalent bonds. The annealing process also causes a portion of the OA ligands to desorb and a corresponding decrease in interparticle spacing (edge-to-edge spacing) between the NCs. High-resolution TEM images (Figure 1 f,g) show that the individual NCs remain isolated from one another before and after the crosslinking procedure and that the ligand matrix remains intact (i.e., the NCs do not sinter together). In addition to localized TEM imaging, we also interrogated the ligand matrix over a large area by using X-ray reflectivity (XRR). By combining these measurements with a geometric model, we conclude that the interparticle spacing between NCs is ≈ 1 nm and ≈ 0.4 nm before and after annealing, respectively (see the Supporting Information).

Gas chromatography–mass spectrometry (GC-MS) data on ligands extracted from the NC surface provides direct evidence of the ligand crosslinking that results from annealing (Figure 2 a). The mass spectra data of the crosslinked ligands
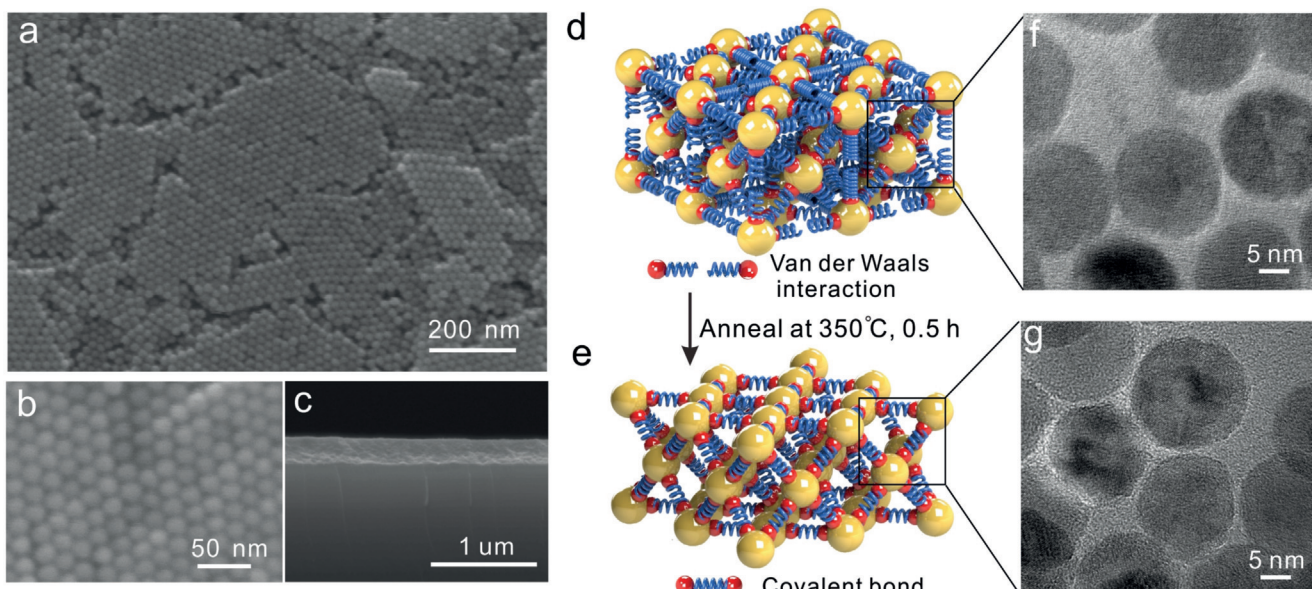

Figure 1. Iron oxide NC thin film characterization before and after ligand crosslinking. a) Scanning electron microscopy (SEM) image of a non-crosslinked iron oxide NC thin film. b) High-resolution SEM image showing that the non-crosslinked iron oxide NCs form ordered assemblies. c) SEM image of the cross-section of an iron oxide NC thin film. Schematic illustrations of d) a non-crosslinked iron oxide NC solid and e) a crosslinked iron oxide NC solid, where the adjacent OA ligands are interacting through weak van der Waals forces and strong covalent bonding, respectively. High-resolution TEM images of f) non-crosslinked and g) crosslinked samples show that the annealing process does not lead to NC sintering.
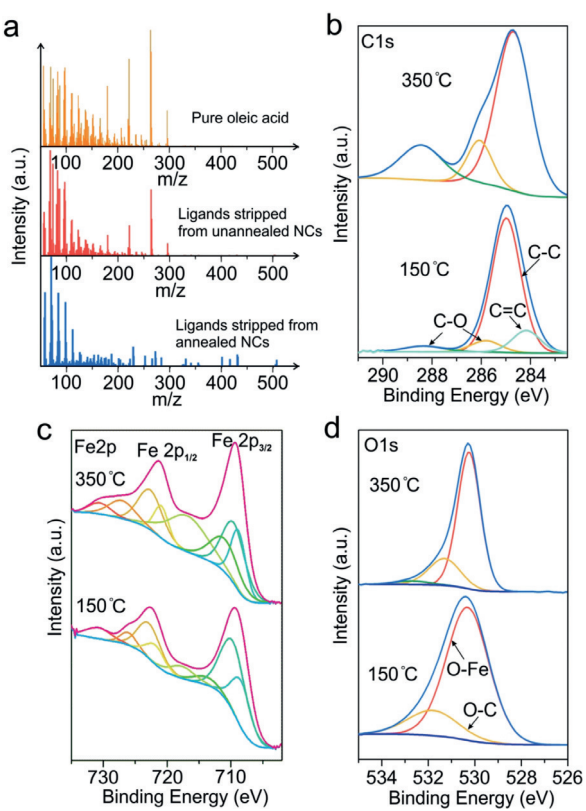
Figure 2. Characterization of ligand crosslinking upon annealing.
a) Mass spectra of pure oleic acid (orange), ligands stripped from NCs prior to annealing (red), and ligands stripped from NCs after annealing (blue). High-resolution X-ray photoelectron spectroscopy scan of b) C1s, c) Fe2p, and d) O1s regions before and after annealing at 350°C.

contain fragments with molecular weights that substantially exceed the molecular weight of OA. This is typically not possible unless the starting material (e.g., crosslinked OA) has a molecular mass exceeding that of OA itself. More specifically, we detect the presence of large m/z peaks (400–500) that are 1.4- to 1.8-times more massive than OA (282). Control measurements on pure OA and non-crosslinked NC solids are identical to each other and distinctly different from the crosslinked ligands. Furthermore, these measurements on control samples do not yield heavy molecular fragments in the 400–500 m/z range that are present in the crosslinked samples.

X-ray photoelectron spectroscopy (XPS) characterization confirms the absence of C=C double bonds in annealed samples and provides additional evidence for OA crosslinking. Figures 2 b–d show high-resolution XPS scans in the C1s, Fe2p, and O1s regions. In the C1s region, a C sp^2 peak is observed at 284 eV that can be attributed to the C=C double bonds in the OA ligands of unannealed NC solids. After annealing at 350°C, the peak corresponding to the C=C double bond disappears. This observation is in agreement with the ligand-crosslinking mechanism described by Dreyer et al.,[7] wherein the C=C double bond splits and forms a new bond that crosslinks adjacent ligands. We identify the strongest peak at 284.8 eV as the aliphatic C atom from the OA molecules. The peaks observed at 286 eV and 288.5 eV

correspond to the carboxylate that binds the OA molecule to the iron oxide NC surface. The annealing process does not induce any notable changes in the peaks of the Fe2p region, indicating that the iron oxide NC cores are not affected by the annealing treatment. The O1s region features two prominent peaks at 530.5 eV and 531.5 eV, which correspond to the lattice oxygen in the iron oxide core and oxygen in the carboxylate that bind the OA molecules to the iron oxide NC surface, respectively. The carboxylate peaks in the C1s and O1s regions remain generally unchanged by the annealing process and indicate that organic ligands remain on the NC surface. The annealing treatment also causes OA ligands that were weakly bound to desorb and a corresponding decrease in the interparticle (edge-to-edge) spacing of the NC solid. We probed this partial desorption of ligands by using thermogravimetric analysis (TGA, Figure S3) and XRR analysis (Section I c in the Supporting Information). Assuming a basic geometric model, uniform ligand coverage, and an absence of unbound ligands, we calculate that the annealing process decreases the organic-ligand capping density from 2 nm^{-2} to 0.8 nm^{-2}. These ligand capping densities are in agreement with prior work by Dreyer et al.[7] and indicate that approximately 40% of the ligands remain on the surface after the annealing treatment that crosslinks the OA ligands.

We measured the cross-plane thermal conductivity of the NC solid films by using the differential 3ω method.[8] Figure 3 a,b is a schematic illustration and cross-sectional SEM image of an NC solid sample that is ready for measurement by the 3ω method (i.e., an NC solid sandwiched by a top SiO$_2$ layer and a bottom Si substrate). A detailed description of our 3ω measurement system can be found in Section II of the Supporting Information and also in our previous work.[5b]

Thermal-transport measurements show that increases in thermal conductivity of up to $\approx 260\%$ accompany the annealing process that crosslinks the NC ligands. Figure 3 d shows the thermal conductivity of non-crosslinked and crosslinked iron oxide NC solids as a function of core diameter at room temperature. The thermal conductivity of non-crosslinked iron oxide NC solids increased from 0.42–0.64 Wm^{-1}K^{-1} as the core diameter increased from 7.9–20 nm. NC solids can be approximated as a nanocomposite consisting of high-thermal-conductivity NC cores embedded in a low-thermal-conductivity ligand matrix. This trend of increasing thermal conductivity with increasing NC diameter is consistent with prior reports,[5] and occurs because the volume fraction of the high-thermal-conductivity component (NC cores) is increasing relative to the low-thermal-conductivity component (ligand matrix). After crosslinking the OA ligands of the NCs, we observed a substantial increase in thermal conductivity for all NC diameters (Figure 3 d). The thermal conductivity of crosslinked iron oxide NC solids increased from 0.81–1.7 Wm^{-1}K^{-1} as the diameter increased from 7.9–20 nm.

Our measured value of 1.7 Wm^{-1}K^{-1} exceeds the highest reported thermal conductivity in a colloidal NC solid by a factor of ≈ 4 (i.e., Liu et al.[5b] measured a thermal conductivity of 0.4 Wm^{-1}K^{-1} for 8 nm diameter PbS NCs with short ethylenediamine ligands). This difference cannot be attributed to a difference in the thermal conductivity of the
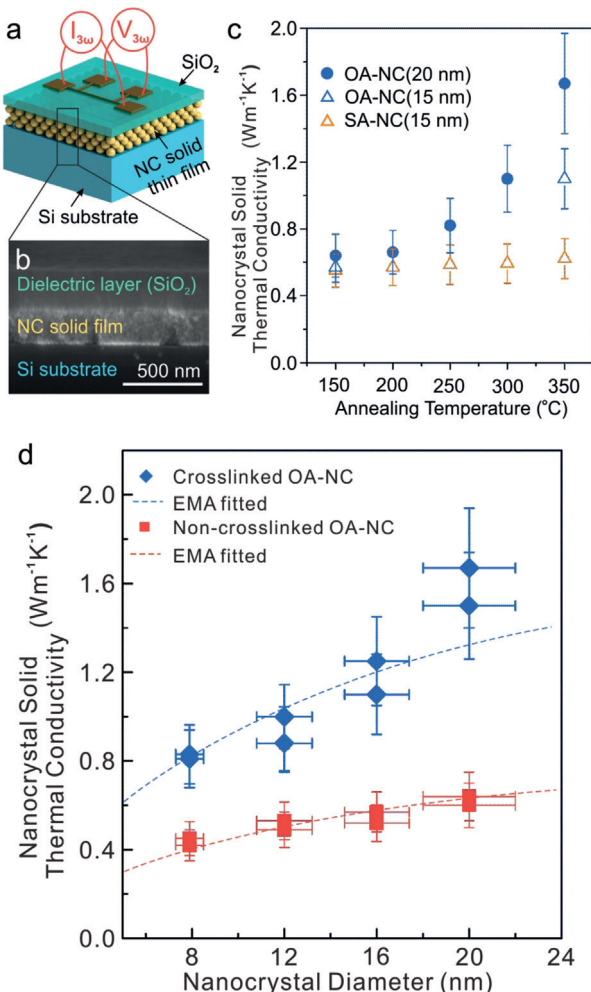
Figure 3. Measurements of thermal conductivity on NC solid films before and after ligand crosslinking. a) Schematic of a sample prepared for thermal-conductivity measurement via the 3ω method. b) Cross-sectional SEM image illustrating the substrate–NC solid film–dielectric SiO₂ stack in the measurement samples. c) Thermal conductivity of oleic acid (OA)-capped NC solids and stearic acid (SA)-capped iron oxide NC solids as a function of annealing temperature for both 15 and 20 nm diameter NCs. d) Room-temperature thermal-conductivity measurements on OA-capped iron oxide NC solids of different NC sizes before and after annealing at 350°C. The dashed lines in d) are fitted results based on an effective medium approximation (EMA) model.

NC cores (Fe₃O₄[9] and PbS[10]) because Ong et al.[5a] showed that thermal conductivity is insensitive to this parameter. The groups of Ong[5a] and Liu[5b] both showed that the NC solid thermal conductivity is directly related to the volume fraction of the ligand matrix. Consequently, a partial explanation for this difference in thermal conductivity is our larger 20 nm NC cores (i.e., smaller volume fraction of the ligand matrix). However, this diameter difference by itself is insufficient to explain the observed difference in thermal conductivity. Our 7.9 nm diameter samples provide a more suitable comparison to the prior work on 8 nm samples by Liu et al.[5b] In this comparison, our measured value of 0.81 Wm⁻¹K⁻¹ is still double that of the value reported by Liu et al.[5b]

Annealing the NC solids with oleic acid in this work leads to two effects, partial ligand desorption and ligand crosslinking, both of which can increase thermal conductivity. Consequently, we performed control experiments using stearic acid (SA) ligands to experimentally confirm that ligand crosslinking is the dominant factor that causes the increased thermal conductivity. SA is chemically identical to oleic acid (OA), except that it lacks the C=C double bond in its carbon backbone. This means that SA ligands cannot crosslink. GC-MS, TGA, TEM, and SEM analysis on SA-capped NCs further confirm that they behave like OA-capped NCs, except for their inability to crosslink (Section I d of the Supporting Information and Figure S5). Consequently, we can use OA ligands to infer the combined effects of ligand crosslinking and partial ligand desorption, whereas we can use SA ligands to infer the effect of partial ligand desorption only.

Figure 3 c demonstrates that ligand crosslinking is the dominant effect that increases thermal conductivity. This figure shows the thermal conductivity of OA-capped and SA-capped NC solids as a function of annealing temperature. For an annealing temperature of 150°C (i.e., a temperature that is too low to induce ligand crosslinking), the thermal conductivity of 15 nm NCs is ≈0.55 Wm⁻¹K⁻¹ regardless of whether OA or SA ligands are used. Beyond this annealing temperature, the thermal conductivities of the OA-capped NC solids rapidly rise, but the thermal conductivities of the SA-capped NC solids increase only slightly. After annealing at 350°C, the thermal-conductivity values for 15 nm NCs reach 1.1 and 0.62 Wm⁻¹K⁻¹ for OA and SA ligands, respectively. Using the OA-case as a proxy for combined ligand crosslinking and ligand desorption, and the SA-case as a proxy for ligand desorption only, we estimate that ligand crosslinking and ligand desorption account for 87% and 13% of the total change in thermal conductivity, respectively.

It is worth noting that our iron oxide diameter series partially overlaps with the iron oxide diameter series studied by Ong[5a] and this provides a means to check the accuracy of our measurements. Our measurement of 0.42 ± 0.08 Wm⁻¹K⁻¹ for 7.9 nm NCs and their measurement of 0.32 ± 0.05 Wm⁻¹K⁻¹ for 8 nm iron oxide NCs are within experimental uncertainty of each other and validate our results. We also investigated the possible effects of sample contact resistance and/or free-electron carriers on our measurements of thermal conductivity, and found that these are negligible (see Sections VII and VIII of the Supporting Information).

To more thoroughly interrogate the origins of our increased thermal conductivity, we performed Young's modulus measurements on the NC solids. According to kinetic theory, thermal conductivity is proportional to sound velocity ($k = 1/3\, C v_s \Lambda$), where k, C, v_s, and Λ are thermal conductivity, volumetric heat capacity, sound velocity, and mean free path of acoustic vibrations, respectively. Furthermore, solid mechanics dictates that sound velocity is proportional to the square root of Young's modulus ($v_{s,ave} \propto \sqrt{E/\rho}$), where $v_{s,ave}$, E, and ρ are the average sound speed, Young's modulus, and density, respectively. Consequently, changes in thermal conductivity can correlate to changes in Young's modulus and vice versa. This relationship has been recognized by other

researchers,[11] and we now use it here to investigate the effects of ligand crosslinking.

We used nanoindentation to measure the Young's modulus of our NC solid films. Figure 4a and b show the indented surfaces of non-crosslinked and crosslinked NC solids, respectively. These SEM images show no pileup of displaced material at the edge of the indent, which allows us to derive the elastic modulus by using the Oliver–Pharr method.[12] We
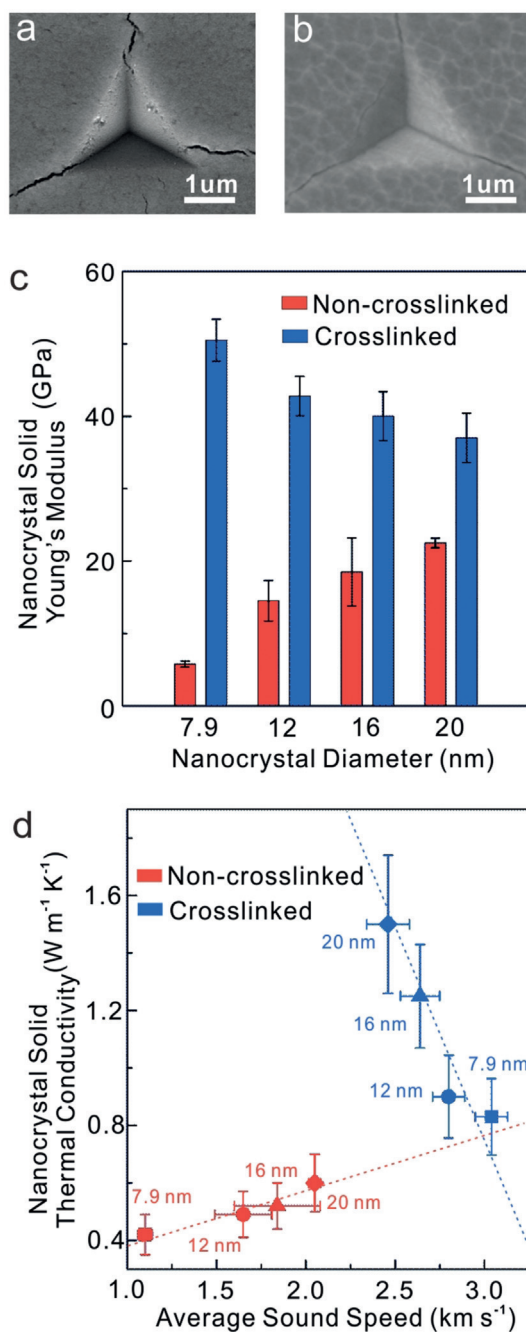
then use Hay's model[13] to subtract the effect of the substrate in our Young's modulus measurements (Figure S8c,d). As shown in Figure 4c, the Young's modulus of the non-cross-linked thin films increases monotonically from 5.75–22.5 GPa as the NC diameter increases from 7.9–20 nm. This trend is due to the decreasing volume fraction of the soft organic ligands and stronger interaction between NC cores,[14] and has been previously observed for OA-capped PbS NC thin films.[15]

In all cases, the Young's modulus of the NC solid increases after ligand crosslinking. The relative change in Young's modulus is greatest for the 7.9 nm diameter NCs, which is intuitive because that sample has the largest volume fraction of ligand matrix. Interestingly, a Young's modulus trend reversal with NC diameter occurs after crosslinking. The Young's modulus of the crosslinked NC solid decreases monotonically from 50.5–36.0 GPa as the core diameter increases from 7.9–20 nm. We speculate that this trend reversal in Young's modulus arises from variations in the effectiveness of the crosslinking procedure as the NC diameter is changed (Section IIIc in the Supporting Information), but also acknowledge that this trend merits further study.

Further dissection of our nanoindentation data allows us to calculate the mechanical properties of the individual components for the NC solid (i.e., NC cores versus ligand matrix). We assume a constant Young's modulus for the iron oxide NC core ($E_{NC} = 163$ GPa)[16] and utilize Halpin–Tsai theory[17] to derive the modulus of the ligand matrix (E_m, Section III in the Supporting Information). The resulting average Young's modulus of the OA ligand matrix is ≈ 0.3 GPa and ≈ 1.8 GPa for non-crosslinked and crosslinked ligand matrices, respectively.

Figure 4d shows that the thermal conductivity of non-crosslinked NC solids is linearly proportional to the average speed of sound in the NC solid. We calculated the average sound speed (one longitudinal and two transversal polarizations) of NC solids by using the Young's modulus from nanoindentations, densities from X-ray reflectivity measurements, and an assumed Poisson ratio of 0.3 (Table S1, S2).[18] Plotting these average sound speeds against NC thermal conductivity reveals a linear proportionality (Figure 4d) that is in line with kinetic theory. Additional analysis shows that changes in heat capacity[19] and/or mean free path do not have meaningful impacts on thermal conductivity as the NC size is changed (Section IV in the Supporting Information). Hence, we conclude that the thermal-conductivity dependence on NC size for non-crosslinked samples is dominated by changes in sound velocity.

The thermal conductivities of crosslinked NC solids exhibit an opposing dependence on average sound speed relative to that of non-crosslinked NC solids (Figure 4d). Rather than increasing linearly with average sound speed, the thermal conductivity of crosslinked NC solids decreases linearly with average sound speed. Kinetic theory predicts a linear proportionality of thermal conductivity to sound speed, volumetric heat capacity, and carrier mean free path. Consequently, this trend in thermal conductivity with sound velocity can only be explained if changes in volumetric heat

Figure 4. Representative SEM images of nanoindented iron oxide NC solids a) before and b) after annealing. c) Young's modulus of non-crosslinked and crosslinked iron oxide NC solids with varying NC core diameter. d) Thermal conductivity of non-crosslinked and crosslinked iron oxide NC solids as a function of derived average sound speed and varying NC core diameter.

capacity and/or carrier mean free path are overpowering changes in sound velocity. As mentioned earlier, changes in volumetric heat capacity are negligible as the NC diameter is varied (Section IVa of the Supporting Information). This indicates that changes in average sound speed are being overpowered by changes in mean free path when it comes to the thermal conductivity of crosslinked NC solids. In short, we conclude that the thermal conductivity of non-crosslinked NC solids is dictated by the speed of sound, whereas the thermal conductivity of crosslinked NC solids is dictated by mean free path.

We further calculate the average sound speed for the ligand matrix by using the modulus derived from the Halpin–Tsai model, the density estimated from geometric modeling, and our XRR data (Section III b of the Supporting Information). The average sound speed of the ligand matrix is calculated to increase from ≈ 600 to $\approx 1700\,\mathrm{m\,s^{-1}}$ for non-crosslinked and crosslinked NC solids, respectively (Table S3). This indicates that acoustic vibrations travel ≈ 2.8 times faster within the crosslinked ligand matrix and naturally leads to an increase in thermal conductivity.

To interpret the effect of the individual NC solid components on the overall NC solid thermal conductivity, we use effective medium approximation (EMA) modeling to fit our thermal-conductivity data (Figure 3d). Thermal interface conductance is an important parameter when modeling the thermal conductivity of nanocomposites, and so we use an EMA model that explicitly accounts for this parameter.[20] The overall NC solid thermal conductivity is then a function of the thermal conductivity of the NC cores (k_{NC}), thermal conductivity of the ligand matrix (k_m), volume fraction of the NC cores (V_{NC}), radius of the NC cores (a), and the core–ligand interface thermal conductance (G). For non-crosslinked OA-capped iron oxide NC solids, we set k_{NC} and k_m to $7\,\mathrm{Wm^{-1}K^{-1}}$ and $0.13\,\mathrm{Wm^{-1}K^{-1}}$ as based on literature values.[5a,9] We utilize the interparticle distance, L, of 1.0 nm from our TEM and XRR data to determine our model input for V_{NC}. We vary G to fit our experimental data and find that $400\,\mathrm{MWm^{-2}K^{-1}}$ yields good agreement (Figure 3d).

To fit our thermal conductivity on crosslinked NC solids, we use the same k_{NC} and G values as the non-crosslinked NC solids. We use the same k_{NC} value because the NC core is unchanged by the crosslinking process. Infrared spectroscopy results also indicate that the ligand-core binding interaction is dominated by the bridging bidentate configuration before and after crosslinking. Consequently, we expect the core–ligand interface conductance, G, to remain the same before and after crosslinking (see Sections I c and V as well as Figures S4 and S14 in the Supporting Information). We change L from 1.0 to 0.4 nm in accordance with our materials characterization data and analysis. The crosslinking process also changes the intrinsic properties of the ligand matrix itself, and so we change k_m from 0.13 to $0.37\,\mathrm{Wm^{-1}K^{-1}}$. This change in k_m was chosen in accordance with the ≈ 2.8-fold change in ligand sound velocity for non-crosslinked and crosslinked ligands mentioned earlier, and the linear proportionality between thermal conductivity and sound velocity dictated by kinetic theory. Figure 3d shows that these rational and simple changes to the EMA model inputs yield reasonable agree-

ment with our experimental data on thermal conductivity for crosslinked NC solids of all diameters.

Our EMA model allows us to decouple the effects of ligand crosslinking and partial ligand desorption on thermal conductivity. Ligand crosslinking and partial ligand desorption occur simultaneously during the sample annealing process, and so decoupling them via modeling provides valuable insight that is difficult to access experimentally. These effects manifest themselves in the EMA model as an increase in k_m and a decrease in L, respectively. Figure 5a shows the relative effects of increasing k_m and decreasing L on NC solid thermal conductivity while all other EMA model parameters remain fixed. The steepness of the k_m curve versus the L curve in Figure 5a indicates that the overall thermal
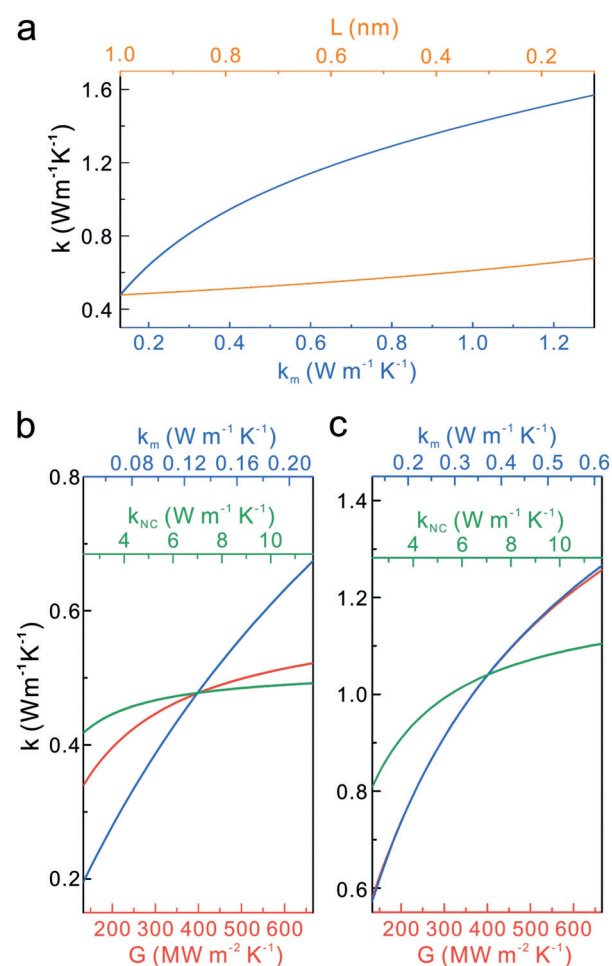

Figure 5. Sensitivity analysis on the effective medium approximation (EMA) model for NC solids with NC cores of 12 nm diameter. a) EMA sensitivity towards k_m (blue) and L (orange). In both curves we hold k_{NC} and G fixed at $7\,\mathrm{Wm^{-1}K^{-1}}$ and $400\,\mathrm{MWm^{-2}K^{-1}}$, respectively. We hold L fixed at 1 nm while varying k_m and we hold k_m fixed at $0.13\,\mathrm{Wm^{-1}K^{-1}}$ while varying L. EMA sensitivity analysis for an NC solid (b) before and c) after annealing towards three independent parameters: k_{NC} (green), G (red), and k_m (blue). Unless a parameter is explicitly varied in part (b), we hold L, k_{NC}, k_m, and G fixed at 1.0 nm, $7\,\mathrm{Wm^{-1}K^{-1}}$, $0.13\,\mathrm{Wm^{-1}K^{-1}}$ and $400\,\mathrm{MWm^{-2}K^{-1}}$, respectively. Unless a parameter is explicitly varied in part (c), we hold L, k_{NC}, k_m, and G fixed at 0.4 nm, $7\,\mathrm{Wm^{-1}K^{-1}}$, $0.37\,\mathrm{Wm^{-1}K^{-1}}$ and $400\,\mathrm{MWm^{-2}K^{-1}}$, respectively.

conductivity of the NC solid is much more sensitive to k_m. Additional EMA analyses are shown in the Supporting Information (Figures S12 and S13a). Based on these EMA analyses, we estimate for 7.9 nm NC solids that changes in k_m and L account for 76% and 24% of the total annealing-induced change in thermal conductivity, respectively. These numbers change slightly as the NC size increases, and for 20 nm NC solids, we estimate that changes in k_m and L account for 85% and 15% of the total change in thermal conductivity, respectively. Compellingly, these EMA predictions are in reasonable agreement with our experimental data on iron oxide NCs with OA and SA ligands (Figure 3c). As discussed earlier, that experimental data indicated that ligand crosslinking and ligand desorption (i.e., changes in k_m and L) account for 87% and 13% of the total change in thermal conductivity, respectively. Consequently, we conclude that ligand crosslinking (and a corresponding change in k_m) is the dominant contributor to the thermal-conductivity increase from annealing.

Although prior work demonstrated that overall thermal transport was dominated by the thermal conductivity of the ligand matrix, this present data on crosslinked NC solids shows that this is no longer the case. Figure 5b shows an EMA sensitivity analysis on a non-crosslinked 12 nm NC solid for varying k_m, G, and k_{NC} values. The center point indicates the nominal values for each of these parameters and the corresponding thermal conductivity of the NC solid. Each input parameter is then varied by a factor of 5 while keeping the other parameters constant. Figure 5b clearly shows that varying k_m leads to the largest changes in overall thermal conductivity and that the effects of varying k_{NC} and/or G are much smaller. This is true for other NC sizes as well (Figure S13b–g) and indicates that the k_m is the bottleneck in thermal transport for non-crosslinked NC solids. This result is in agreement with prior work.[5] Figure 5c shows a similar sensitivity analysis, but instead considers crosslinked samples. In this case, the effects of varying G and k_m values are nearly identical. Consequently, meaningful increases in thermal conductivity should be achievable by either increasing the interface conductance at the NC–ligand interface or by increasing the ligand-matrix thermal conductivity itself. Interestingly, Figure 5c also shows that changing k_{NC} could now lead to detectable changes in overall thermal conductivity (whereas changing this parameter in non-crosslinked NC solids has a near-negligible effect). These trends also hold for other NC sizes (Figures S13b-g).

Lastly, we performed molecular dynamics (MD) simulations on two simplified models of NC solids to investigate the effect of crosslinking (Section VI of the Supporting Information). This analysis shows that given the same steady-state heat flux, the magnitude of the temperature gradient in the NC solid with van der Waals ligand interactions is much greater than the NC solid with a covalent bond between ligands (Figure S15). This indicates that the NC solid with covalent bonding has a higher thermal conductivity. We next focused on the temperature distribution along a single NC pair and the ligand molecules between them (Figure S16). In the van der Waals ligand interactions, there is a sharp drop in temperature at the ligand–ligand interface. This indicates that the ligand–ligand interface is the thermal-transport bottleneck, and is in agreement with the findings of our prior work.[5b] After exchanging the van der Waals interaction with a covalent bond, the temperature drop across the ligand–ligand interface substantially diminishes, which is indicative of a large increase in thermal conductivity of the NC solid. These MD simulations corroborate our earlier conclusions that ligand crosslinking substantially increases thermal conductivity.

Conclusion

We used a combination of materials characterization, thermal-transport measurements, mechanical measurements, and modeling to show that ligand crosslinking significantly increases thermal transport in colloidal NC solids. This work also demonstrates that thermal transport in non-crosslinked NC solids is primarily controlled by the speed of sound, whereas thermal transport in crosslinked NC solids is primarily controlled by the mean free path of acoustic vibrations. This work sheds light on ligand design for thermal transport in NC solids. This knowledge will play an important role in NC solid devices where thermal transport can crucially effect device performance and lifetime (e.g., electronics, optoelectronics, and photovoltaics). Future studies on additional crosslinking chemistries to boost thermal transport would also be interesting. For example, molecular crosslinking can be achieved via non-thermal means, such as exposure to UV light.[21] These approaches could greatly expand the applicability of ligand crosslinking to systems beyond the iron oxide–OA ligand system studied in this work.

Conflict of interest

The authors declare no conflict of interest.

[1] a) D. V. Talapin, J. S. Lee, M. V. Kovalenko, E. V. Shevchenko, *Chem. Rev.* **2010**, *110*, 389–458; b) J. S. Lee, M. V. Kovalenko, J. Huang, D. S. Chung, D. V. Talapin, *Nat. Nanotechnol.* **2011**, *6*, 348–352; c) S. J. Oh, Z. Q. Wang, N. E. Berry, J. H. Choi, T. S. Zhao, E. A. Gaulding, T. Paik, Y. M. Lai, C. B. Murray, C. R. Kagan, *Nano Lett.* **2014**, *14*, 6210–6216.

[2] R. Saran, R. J. Curry, *Nat. Photonics* **2016**, *10*, 81–92.

[3] a) J. Tang, K. W. Kemp, S. Hoogland, K. S. Jeong, H. Liu, L. Levina, M. Furukawa, X. H. Wang, R. Debnath, D. K. Cha, K. W. Chou, A. Fischer, A. Amassian, J. B. Asbury, E. H. Sargent, *Nat. Mater.* **2011**, *10*, 765–771; b) M. J. Yuan, M. X. Liu, E. H. Sargent, *Nat. Energy* **2016**, *1*, 16016.

[4] R. Y. Wang, J. P. Feser, J. S. Lee, D. V. Talapin, R. Segalman, A. Majumdar, *Nano Lett.* **2008**, *8*, 2283–2288.

[5] a) W.-L. Ong, S. M. Rupich, D. V. Talapin, A. J. McGaughey, J. A. Malen, *Nat. Mater.* **2013**, *12*, 410; b) M. Liu, Y. Ma, R. Y. Wang, *ACS Nano* **2015**, *9*, 12079–12087.

[6] W. Y. William, J. C. Falkner, C. T. Yavuz, V. L. Colvin, *Chem. Commun.* **2004**, 2306–2307.

[7] A. Dreyer, A. Feld, A. Kornowski, E. D. Yilmaz, H. Noei, A. Meyer, T. Krekeler, C. Jiao, A. Stierle, V. Abetz, *Nat. Mater.* **2016**, *15*, 522.

[8] a) T. Borca-Tasciuc, A. Kumar, G. Chen, *Rev. Sci. Instrum.* **2001**, *72*, 2139–2147; b) D. G. Cahill, *Rev. Sci. Instrum.* **1990**, *61*, 802–808; c) S. M. Lee, D. G. Cahill, *J. Appl. Phys.* **1997**, *81*, 2590–2595.

[9] G. A. Slack, *Phys. Rev.* **1962**, *126*, 427–441.

[10] Y.-L. Pei, Y. Liu, *J. Alloys Compd.* **2012**, *514*, 40–44.

[11] a) T. T. Jia, G. Chen, Y. S. Zhang, *Phys. Rev. B* **2017**, *95*, 143515; b) G. A. Elbaz, W.-L. Ong, E. A. Doud, P. Kim, D. W. Paley, X. Roy, J. A. Malen, *Nano Lett.* **2017**, *17*, 5734–5739; c) M. B. Zanjani, J. R. Lukes, *J. Appl. Phys.* **2014**, *115*, 143515.

[12] W. C. Oliver, G. M. Pharr, *J. Mater. Res.* **1992**, *7*, 1564–1583.

[13] J. Hay, B. Crawford, *J. Mater. Res.* **2011**, *26*, 727–738.

[14] S. M. Rupich, E. V. Shevchenko, M. I. Bodnarchuk, B. Lee, D. V. Talapin, *J. Am. Chem. Soc.* **2010**, *132*, 289–296.

[15] P. Podsiadlo, G. Krylova, B. Lee, K. Critchley, D. J. Gosztola, D. V. Talapin, P. D. Ashby, E. V. Shevchenko, *J. Am. Chem. Soc.* **2010**, *132*, 8953–8960.

[16] H. J. Reichmann, S. D. Jacobsen, *Am. Mineral.* **2004**, *89*, 1061–1066.

[17] J. C. H. Affdl, J. L. Kardos, *Polym. Eng. Sci.* **1976**, *16*, 344–352.

[18] L. E. Kinsler, *Fundamentals of acoustics*, 4th ed., Wiley, New York, **2000**.

[19] a) D. H. Huang, S. L. Simon, G. B. McKenna, *J. Chem. Phys.* **2005**, *122*, 084907; b) X. Xie, D. Y. Li, T. H. Tsai, J. Liu, P. V. Braun, D. G. Cahill, *Macromolecules* **2016**, *49*, 972–978; c) C. L. Snow, Q. A. Shi, J. Boerio-Goates, B. F. Woodfield, *J. Phys. Chem. C* **2010**, *114*, 21100–21108; d) S. Harikrishnan, S. Kalaiselvam, *Thermochim. Acta* **2012**, *533*, 46–55.

[20] D. Hasselman, L. F. Johnson, *J. Compos. Mater.* **1987**, *21*, 508–515.

[21] A. Nsubuga, K. Zarschler, M. Sgarzi, B. Graham, H. Stephan, T. Joshi, *Angew. Chem. Int. Ed.* **2018**, *57*, 16036–16040; *Angew. Chem.* **2018**, *130*, 16268–16272.